Article

Mesoscale Shoreline Evolution on a Carbonate Sand Island: Anegada, British Virgin Islands

Anna Lisa Cescon [1], J. Andrew G. Cooper [1,2,*], Derek W. T. Jackson [1,2], Antoine Collin [3]
and Shannon Gore [4]

1 School of Geography and Environmental Sciences, University of Ulster, Coleraine BT52 1SA, UK;
d.jackson@ulster.ac.uk (D.W.T.J.)
2 Geological Sciences, University of KwaZulu-Natal, Durban 4000, South Africa
3 Laboratoire de Géomorphologie et Environnement Littoral, École Pratique de Hautes Études,
35800 Dinard, France
4 Coastal Management Consulting, Road Town, Tortola VG1110, UK
* Correspondence: jag.cooper@ulster.ac.uk

Abstract: Anegada, the easternmost island of the Virgin Islands group (Caribbean Sea), is a low Pleistocene carbonate platform surrounded by Horseshoe Reef, the world's third-largest fringing reef. The western part of the island consists of an extensive beachridge plain (>40 ridges). The sandy carbonate shoreline exists in three morphodynamic domains that exhibit distinctive behaviour over the 59-year study period (1953 to 2012). The northern shore is dominated by westerly longshore drift under fair-weather conditions and cross-shore sediment transport during high-energy events. Storm wave run-up and high nearshore sediment availability contribute to the construction of shore-parallel beachridges. The western end of the island is affected by refracted waves that drive strong erosion and sediment transport. This is reflected in a succession of alternating rapid shoreline recession and progradation phases over the study period. The south–central shoreline is exposed to low wave energy and is stable and colonised by mangroves. The fringing reef plays a dominant role in mesoscale shoreline morphodynamics, both as a sediment source and in wave energy dissipation. Quasi-stable points and embayments suggest a strong influence of the reef framework in controlling the shoreline's morphology and position. Sediment transfer from the reef to the shoreline appears to take place via shore-oblique, linear sediment transport pathways that develop across the lagoon in response to the modification of incoming waves. Cannibalisation of the shoreline sediment over the past 50 years is leading to straightening of the shoreline planform. This is counter to the long-term (Holocene) development of beachridges and suggests a change from a strongly positive to negative sediment budget.

Keywords: coral reef; extreme wave events; shoreline change analysis; beachridge; carbonate beach

1. Introduction

The behaviour of dynamic sandy shorelines on reef islands reflects the interaction of sediment supply and nearshore processes [1,2]. They are thought to be particularly sensitive to sea-level changes [3], variations in the productivity of the coral reef [4], and natural wave variability, including swell events, storms, and tsunamis [5]. Their persistence in a global climate change context is essential for many nations globally [6]. Understanding their mesoscale evolution (over years to decades and from 1 to 100 km in scale [7]) helps in the understanding of their response to gradual changes and extreme events.

Biological productivity is the dominant factor in sediment supply on most reef islands [4], but sediment can also be derived from the erosion of pre-existing carbonate deposits [5]. As coral reefs' survival is threatened by climate change, future nearshore processes on these islands may differ strongly from the present [4]. Since 1970, coral bleaching and mass mortality events have increased in frequency and extent [6]. It has been

conjectured that the global decline of coral reefs will increase the exposure of sandy coasts in hurricane-prone areas that currently benefit from the protection of such reefs [8,9]. In contrast to their sheltering effect, however, reefs can also trap extreme waves in the lagoon, leading to an intensification of damage on the beach [10]. A better understanding of the mesoscale behaviour of sandy shorelines on reef islands is therefore essential.

This paper documents the mesoscale shoreline evolution of the mobile sandy shorelines of western Anegada, a reef-top island in the eastern Caribbean, and interprets these changes in the context of nearshore processes and, in particular, the respective roles of fair-weather and extreme waves. The results add to the understanding of multidecadal shoreline changes on reef islands that are widely believed to be threatened by ongoing and near-future sea-level rise [11–13], and whose sediment supply is intimately linked to changes on the adjacent reefs [1,14–16].

2. Study Site

Anegada is the easternmost island of the British Virgin Islands (BVI), situated between the Greater Antilles platform and the Atlantic Ocean [17] (Figure 1). Its name (anegada = flooded in Spanish) derives from its low topography and the presence of island-top ponds, rendering it a flooded or drowned appearance. Its long axis runs from east to west, and the shoreline is approximately 37 km, of which 16 km is backed by a beachridge plain. The remainder is an emergent reef platform with a hard, rocky coast of emergent reef material. The island stretches from west to east over 17 km and is, on average, 4 km wide (Figure 2). The highest elevation is 8 m above sea level [18]. The island comprises an elevated Pleistocene carbonate platform in the east, while the west comprises a beachridge complex [17] with salt pans. Mangroves are present along the southeast shoreline. The bathymetry around Anegada is marked by a strong contrast between the steep Atlantic-facing northern and the low-gradient Caribbean-facing southern shorelines (Figure 2).
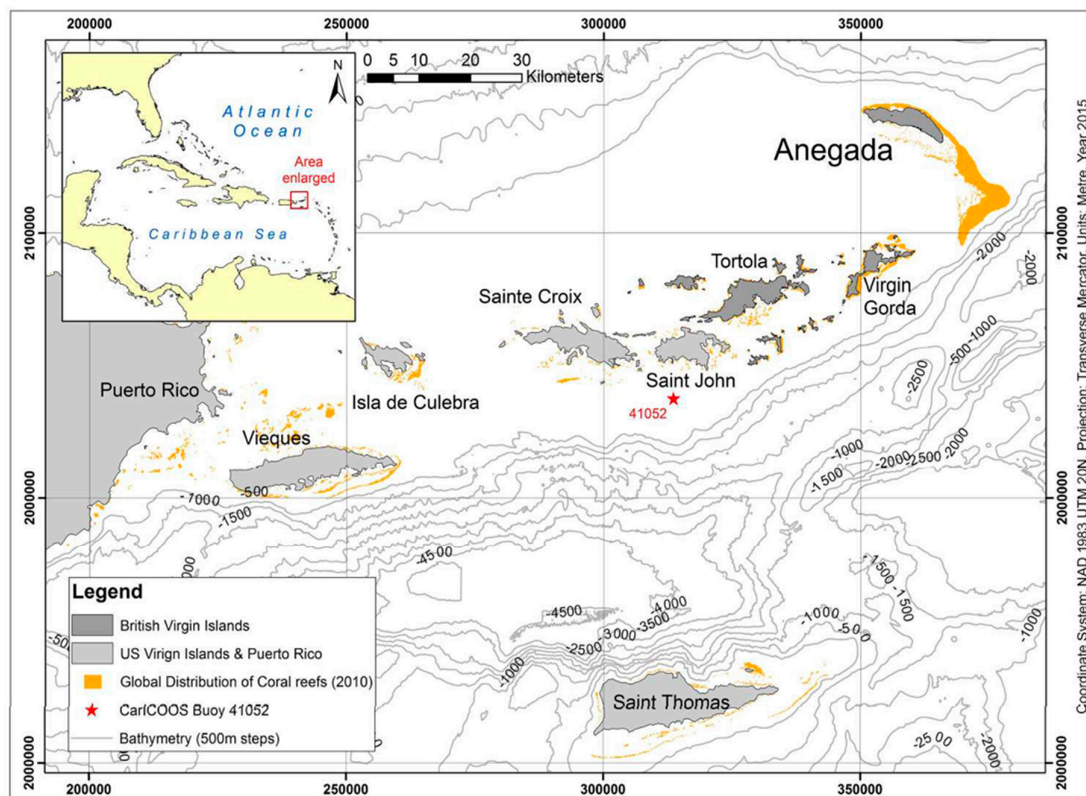

Figure 1. Geographical setting of the Virgin Island group and the island of Anegada. The bathymetry is displayed in 500 m intervals. The position of CariCOOS Buoy 41052 is shown.
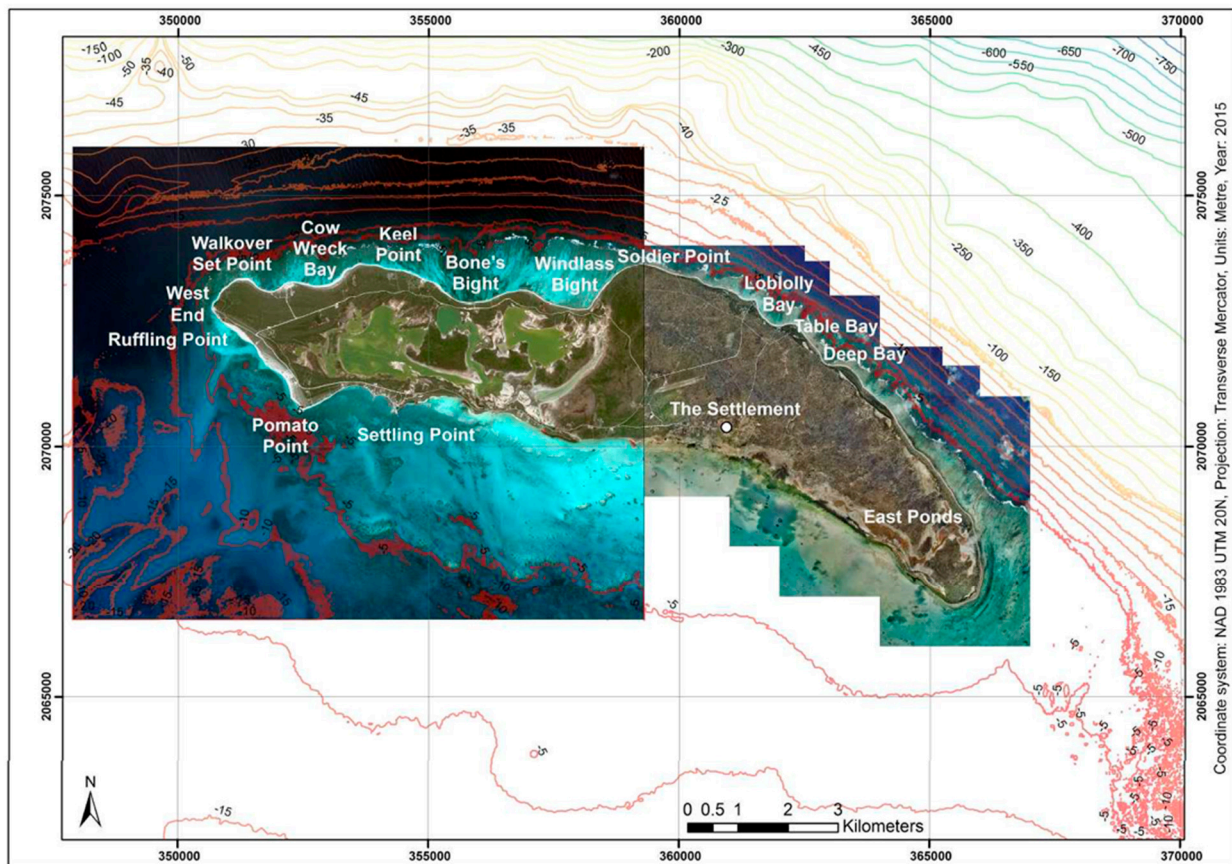
Figure 2. Anegada island and the surrounding bathymetry. The western side is represented by a 2009 GeoEye-1 satellite image (5 m resolution, natural colours), while the eastern part is represented by the 2002 aerial photo set (10 m resolution). Combined bathymetry originates from this study. The isobaths have a 5 m step for 0 to 50 m, and then a 50 m step for the deeper values.

The island's climate [19] is dominated by the northeast trade winds and is classified as Aw in the Köppen classification [20]. Outside hurricanes and tropical storms, wind speeds seldom exceed 9 ms^{-1}. The hurricane season extends from June to November, and these generally approach Anegada from the southeast. The temperature varies little through the year, with daily maxima ranging from 25 to 29 °C and minima from 19 to 23 °C. Rainfall averages 890–1000 mm/year and is concentrated in October and November.

The sandy beachridge plains of Anegada have long been known [17,18,21], but no systematic analysis of shoreline changes has been undertaken to date. The northern, Atlantic-facing plain has at least 25 beachridges, while the southern, Caribbean-facing plain contains about 15 ridges. Both sets are composed of well-sorted, well-rounded to sub-rounded carbonate sands [22,23]. These beachridges enclose hypersaline ponds [18,22,24]. Breaches in the beachridges along the northern shore have been attributed to historical tsunami waves [25,26].

The Horseshoe Reef (Figures 1 and 2) forms a fringing barrier along the northern shore of Anegada and is present as patch reefs in the south [18]. It is the source of clastic carbonate sediments on Anegada. Horseshoe Reef is categorised as "at-risk" or threatened" [27]. Caribbean islands experience extreme waves of three types: ground swells generated by distant storms [28], extreme storm or hurricane waves [25,29], and tsunami waves [5,21]. Anegada is dominated by easterly trade winds, and a near-unidirectional easterly wave direction on its Atlantic coast (Figure 3) [17] generates a strong longshore drift. Tsunami waves have been recorded in the BVI [30], and tsunami deposits identified in the central part of Anegada [21,31] have been tentatively dated to post-1650 AD [32] and 1200 to 1500 AD [33].
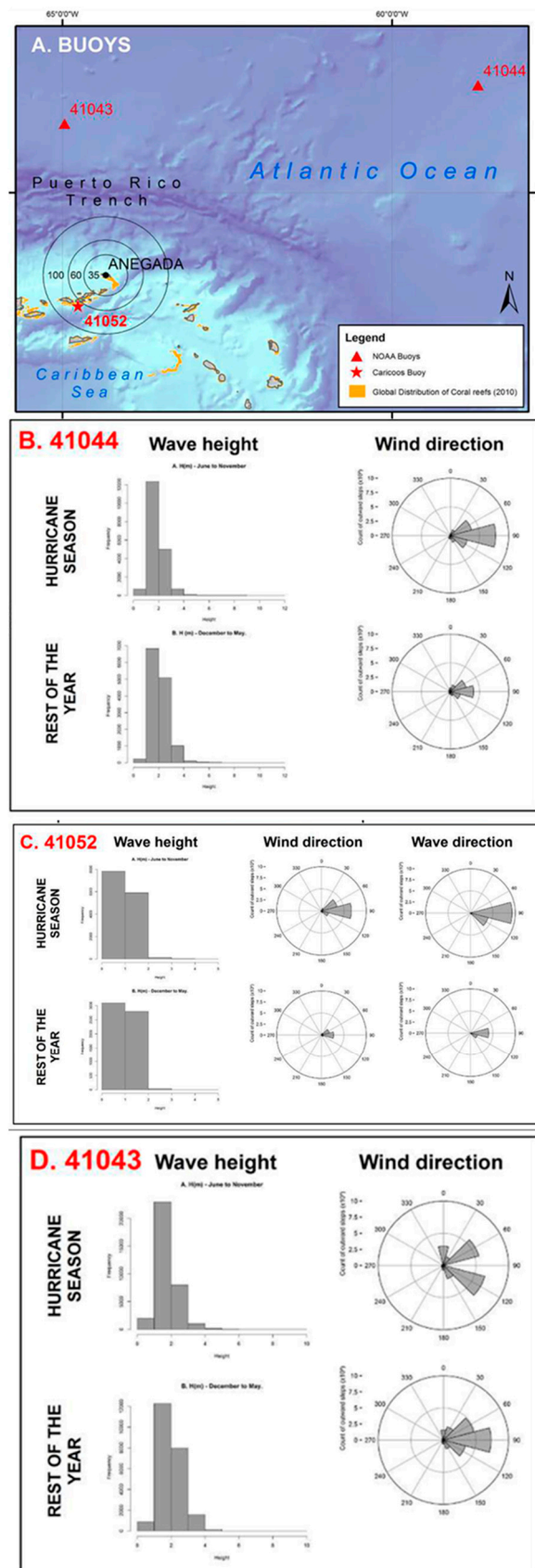
Figure 3. Wave height, wind direction, and wave direction retrieved from the three buoys: (**A**) Position of the buoys relative to the island of Anegada [34]. (**B**) Buoy 41044, northeast of Saint Martin. (**C**) Buoy 41052, south of Saint John. (**D**) Buoy 41043, northeast of Puerto Rico.

3. Methods

Fieldwork in November 2012 and February 2015 involved GPS and DGPS mapping, as well as sediment sampling along the entire western coastline from Soldier Point to Settling Point (Figure 2). Standard meteorological data were sourced from the US National Oceanic and Atmospheric Administration (NOAA) buoys archive [35] (Table 1, standard meteorological data). Two NOAA buoys were used to characterise the Atlantic wave climate: buoy 41043 and buoy 41044, 266 km northwest and 673 km northeast of the island, respectively. Buoy 41052 of the CariCOOS (Caribbean Coastal Ocean Observing System) network, 68 km southwest of the island, was used to characterise the Caribbean Sea waves. Monthly averages were compiled and differences between hurricane season (June to November) and non-hurricane season (December to May) were considered. Extreme wave events (swell, storm, and hurricane events) were identified as described by Cooper et al. [28].

Table 1. Data used in the study.

Data	Date	Description					Source
Fieldwork	2012 and 2015	Fieldwork observations.					This work
		The sets have a range of preservation quality; 1953 to 1992 are scanned and rectified					
			Agency	Mission name	Altitude (feet)	Number of tiles	Number of tiles used	
Aerial photos	1953		RAF	Leeward Islands N. 9	2500	26	23	DDM (BVI)
	1959		USAF	VM 88 1372MCS	5000	6	5	
	1966		RAF	//	5000	18	16	
	1969		//	103-VI-2 ANEGADA	6250	20	17	
	1992		Geomatics	LWI92-011	2000	22	20	
	2002		//	//	//	90	90	
Satellite image	2009	GeoEye-1 image in panchromatic (0.5 m resolution) and 4 colour bands (blue to infrared, 2.5 m resolution)					GeoEye
Standard meteorological data	Accessed 2014	Wind and wave data collected from 3 different buoys over different periods from 2007 and 2013					NOAA
Hurricane tracks	Accessed 2015	Storms and hurricanes are listed per season for the North Atlantic; wind speed gives the classification on the Saffir–Simpson scale					NOAA
Bathymetry data	2012	NOAA US Virgin Islands DEM from 2012 (Grothe et al., 2012 [36])					NOAA
	Various	BVI nautical charts					BVI Govt.
	2013	Bathymetric survey of Anegada (unpublished)					BVI Govt.

Table 1. *Cont.*

Data	Date	Description	Source
LiDAR	Terrestrial 21 January 2014	Bare-earth terrain model by Quantum Spatial for the Puget Sound Lidar Consortium; Optech Orion M300 sensor system; Cessna 210 Caravan aircraft Fredericks, X., ten Brink, U.S., Atwater, B.F., Kranenburg, C.J., Nagle, D.B., 2016, Coastal Topography—Anegada, British Virgin Islands, 2014: U.S. Geological Survey data release, http://dx.doi.org/10.5066/F7GM85F3	USGS
	Marine 19–20 March 2014	LiDAR survey led by C. Wayne Wright, USGS; Experimental Advanced Airborne Research Lidar, version B, emitting three simultaneous 532 intervals; Cessna 310 aircraft; nanometre laser pulses at 700 picoseconds	
Benthic habitats	1992	Shapefile of the benthic habitats of the BVI	BVI Govt.

Storm and hurricane events that have affected Anegada since 1851 were extracted from the NOAA database [37] (Table 1, hurricane tracks) and processed within ArcGIS v.10.1. As described by Gardner et al. [34], three "buffer" zones were created, of 30 km diameter for storm events up to hurricane category 2, 60 km for category 3, and 100 km for categories 4 and 5. A list of the storm and hurricane events that have affected Anegada was then compiled. These climatic and wave data informed the subsequent wave modelling.

Wave modelling was used to simulate the wave dynamics around Anegada under various scenarios. A combined bathymetry grid was produced in ArcGIS from five different data sources (Table 1). The base grid was from the NOAA US Virgin Islands DEM of 2012 [36]. Combined bathymetric surveys around Anegada [38] and digitised nautical charts were used to create a general bathymetry for the Virgin Islands Bank. Finally, terrestrial and marine LiDAR data collected by the BVI government and USGS in 2013 and 2014 were used to build a 10 m resolution grid for Anegada and part of Horseshoe Reef. To extend the bathymetric grid along the shallow southern lagoon, relative bathymetry [39] was extracted from a 2.5 m high-resolution 2009 GeoEye-1 multispectral satellite image, using the 2013 bathymetry survey and the 2014 LiDAR survey as control points. Only the southern part of the satellite image was selected for this study, as the extracted bathymetry in the northern part overlaps the 2014 marine LiDAR. This procedure extended the combined bathymetric grid over the patch reefs near Pomato Point. The 2.5 m relative bathymetry was resampled at 10 m and merged with the pre-existing 10 m resolution grid.

In the absence of in situ wave measurements, synthetic wave events were modelled for a range of wave and wind conditions as described by Loureiro et al. [40] using SWAN, a third-generation wave model [41]. Significant wave height and wave direction were simulated to provide an insight into wave-induced sediment transport potential and help in the interpretation of observed historical shoreline changes.

Wave conditions were modelled with a four-step nested workflow using a regional 50 m grid (57×39 km^2), a 20 m grid (33×23 km^2), a 15 m grid (29×17 km^2), and an island-scale 10 m grid (23×13 km^2). The synthetic storm approach used the wind and wave data tabulated in Table 2. Fair weather, swells, and specific storms and hurricane wave conditions were simulated for seven sets of initial wind and wave data (Tables 3 and 4). The hydraulic roughness of coral reefs is difficult to estimate [42]. Consequently, the Madsen bottom friction of reef areas varied from low (0.25 m) to high (1.8 m) [43]. The bottom friction for other benthic habitats was also added as follows: sand and muds (0.08 m [44]), algae (0.1 m [44]), seagrass (0.2 m [45]), and coral rubble (0.12 m [44]).

Table 2. Wave and wind input parameters for the different wave models.

Storm Event	Physical Inputs	Parameters	-		
	Wave Height (m)	Wave Period (s)	Wave Direction (Nautical Degrees)	Wind Speed (m.s^{-1})	Wind Direction (Nautical Degrees)
Fair weather	1.8	6	90	6	100
Swell	4	8	130	8	110
TD Eloise	3	7	90	15	90
H1 Debby	5	7	90	33.5	135
H1 Omar	5	7	200	24	200
H3/H4 Earl/Hugo	10	10	90	56	90
H4 Donna	12	12	110	66	110

Table 3. Physical settings for SWAN model runs.

Storm Event	Water Level (m)	Physics—Run				
		GEN 3	WCAPping	QUADruplets	WINDGrowth	FRICtion
Fair weather	0.5	JANSSEN	OFF	OFF	OFF	MADsen
Swell	0.5	JANSS EN	OFF	OFF	OFF	MADse n
TD Eloise	1	JANSSEN	OFF	OFF	OFF	MADsen
H1 Debby	1	JANSSEN	OFF	OFF	OFF	MADsen
H1 Omar	1	JANSSEN	OFF	OFF	OFF	MADsen
H3/H4 Earl/Hugo	1	JANSSEN	OFF	OFF	OFF	MADsen
H4 Donna	1	JANSSEN	OFF	OFF	OFF	MADsen

Table 4. Diffraction settings for SWAN model runs.

Storm Event	DIFFRACtion			
	50 m	20 m	15 m	10 m
Fair weather	Yes	Yes	Yes	Yes
Swell	Yes	Yes	Yes	Yes
TD Eloise	Yes	Yes	Yes	Yes
H1 Debby	Yes	Yes	Yes	Yes
H1 Omar	Yes	Yes	Yes	Yes
H3/H4 Earl/Hugo	Yes	Yes	No	No
H4 Donna	Yes	No	No	No

Shoreline change analysis was undertaken using historical aerial photos and high-resolution satellite images (Table 1) spanning from 1953 to 2009. The shoreline is clearly identifiable both as the high-water mark (HWM) [46] and the vegetation line [47,48]. The 2002 orthophoto set was available in a digital georeferenced format. The remaining aerial

photos were digitised at 1200 dpi and rectified within ER Mapper v.7.2 using the 2002 aerial photoset as a reference for an NAD83-UTM20N geographical projection. Because western Anegada shows little topographic variation, triangulation was used for image rectification [49]. Ground control points included roads, buildings, and distinctive coral patches. A few photos were discarded due to poor quality, clouds and their shadows, a limited number of ground control points (Table 1). Some of the photos with partial cloud cover were rectified because enough control points were visible, but the obscured surface was excluded from further analysis. The HWM and vegetation line were digitised from 1953 to 2009 within ArcGIS 10.1. Some of the digitised shorelines were discontinuous due to the quality of the imagery. The rectification error for digitised shorelines increases with increasing age: the error is 10 m for 1953 and 1959, 5 m for 1966 and 1969, and 2.5 m for 1992.

The Digital Shoreline Analysis System v. 4.0 (DSAS [50]) was used to analyse historical coastal changes. Shapefiles containing the HWM and vegetation lines were created. Shoreline transects were built at 10 m intervals to mirror possible variations in the lagoon's bathymetry. The net shoreline movement (NSM), shoreline change envelope (SCE), and end point rate (EPR) were calculated and then collated within ArcGIS.

Results are presented for the north and west coasts (1953–2009) and the south coast (1959–2009). Six change intervals between successive HWM shoreline records are covered: 1953–1966, 1959–1966, 1966–1969, 1969–1992, 1992–2002, and 2002–2009. For ease of description, changes were considered for nineteen coastal sections: eight on the northern shore and eleven on the southern shore.

4. Results

4.1. Coastal Geomorphology

The north-facing sandy shoreline from Soldier Point to West End is exposed to wind-generated waves predominantly moving from east to west, and also to ocean swells. The sandy shoreline, however, is sheltered from direct wave impacts by a wide lagoon and a reef crest. At the southwest end of the island (West End to Pomato Point), the shoreline changes orientation and is not sheltered by an offshore reef. This stretch is affected by refracted wind waves and swells that progressively lose energy as they enter the Caribbean Sea. The low-energy southern shoreline is colonised by mangroves and lacks a well-developed sand beach.

Soldier Point marks the contact between the lithified last interglacial section of the island to the east [25,51] and the unconsolidated Holocene-to-recent beachridge section to the west. Soldier Point is exposed to persistent energetic waves [52], and coral clasts and limestone boulders are scattered over the rock platform. There is little sand, and shrubby vegetation covers a boulder, pebble, and clast coral ridge in the backshore [52]. To the west, a continuous sandy beach extends for over 9 km along the northern shoreline. This is backed by multiple beachridges topped with windblown sand. Occasional, small outcrops of beachrock constitute the only lithified units on this stretch of coast. The planform of the modern sandy shoreline comprises a series of temporally persistent sandy points and intervening embayments (Figure 1). The reef crest extends continuously along the northern coast and is located between 0.3 and 1.3 km seaward of the beach. The seaward face of the beachridges shows variable topography. On prominent points (e.g., Keel Point and Ruffling Point), recent erosional scarps were present during surveys in 2012 (Figure 4A), while along most of the coast the ridges slope gently to the upper beach (Figure 4B). The beach face is typically 10 m wide from the base of the landward ridge to the water's edge. It is steep and terminates seaward in a well-defined beach step. The beach sands are entirely composed of biogenic grains that are typically well-rounded and moderately–well-sorted [23]. The beach step abuts a shallow subtidal area mantled by fine mud. In the 2012 survey, small shell fragments and fresh seaweed with occasional broken coral clasts were scattered on the beach berm. They were mainly from *Acropora palmata* (elkhorn coral) and *Acropora cervicornis* (staghorn coral), and they probably originated during Hurricane Sandy swells.
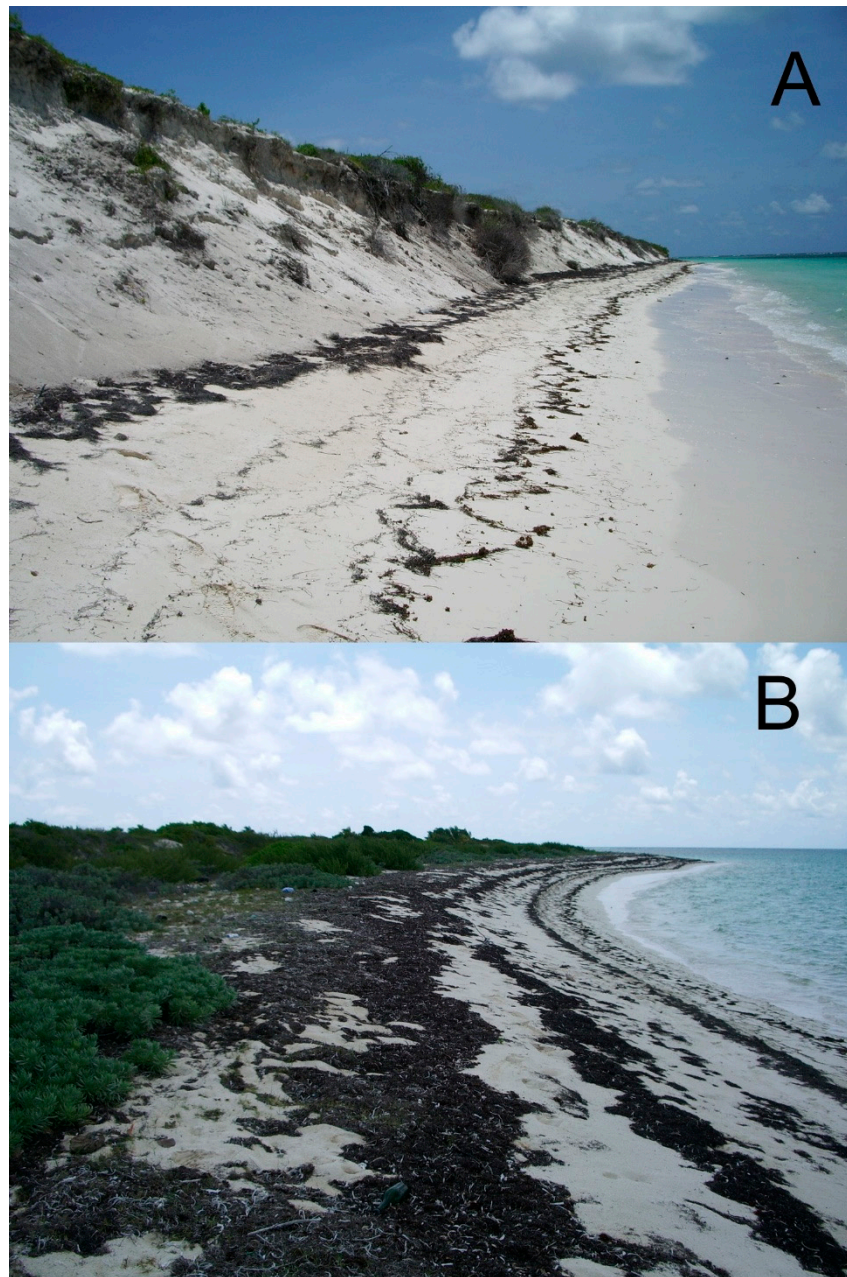
Figure 4. Ground photographs of the eroding (**A**) Keel Point and accreting (**B**) Pomato Point sectors of the carbonate sandy shoreline of Anegada; for locations, see Figure 2.

At the southwest end of the island, the shoreline's orientation changes abruptly, although the continuous sandy beach continues for a further 4 km. Unlike the north-facing beach, this section is fronted by shallow subtidal sand flats colonised by seagrass. The beach planform here also comprises alternating points and embayments that are temporally persistent. It is backed by a series of beachridges with less dense vegetation than those of the northern shoreline.

4.2. Climate and Wave Environment

Wind and wave data are presented in Figure 3 and Table 5. Swell events were extracted from the three buoy records (Figure 3). No wave height over 4 m lasting more than 6 h was recorded for the Caribbean buoy for the period 2011 to 2013. Twenty swell events (period > 6 s) unrelated to hurricanes were recorded for buoy 41043 between 2007 and 2013. Sixteen swell events were recorded at buoy 41044 between 2010 and 2013.
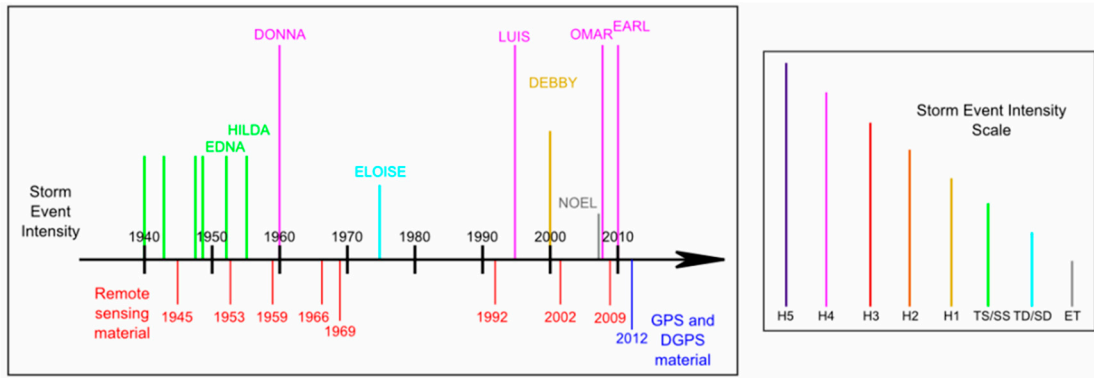
Table 5. Average wave and wind conditions for the three buoys.

Average All Data	Hsig (m)	Dir (deg)	T (s)	Wind (m/s)	Wind Dir (degT)
Northeast Puerto Rico (41043)	1.82	91.80	5.91	6.28	101.68
Northeast Saint Martin (41044)	1.93	81.41	6.16	6.17	106.17
South Saint John (41052)	1.04	103.14		6.08	88.07
Hurricane season	Hsig (m)	Dir (deg)	T (s)	Wind (m/s)	Wind Dir (degT)
Northeast Puerto Rico	1.68	92.74	5.72	6.17	103.95
Northeast Saint Martin	1.79	91.46	5.90	6.21	103.10
South Saint John	1.01	104.65		5.98	93.35
Out of hurricane season	Hsig (m)	Dir (deg)	T (s)	Wind (m/s)	Wind Dir (degT)
Northeast Puerto Rico	1.97	90.54	6.12	6.41	99.36
Northeast Saint Martin	2.08	61.32	6.42	6.13	109.24
South Saint John	1.08	101.33		6.20	81.74

Using the hurricane influence areas approach [34], 28 storm and hurricane events were identified since 1852 (Figure 5). They varied from extratropical storms (ET) to category 4 hurricanes. Fifteen of these impacted Anegada from 1940 to 2010 (Figure 6), encompassing the period for which shoreline data are available. In the 1940s and 1950s, six tropical storms were recorded. Then, Hurricane Donna (category 4) in 1960 was followed by a quiet period of 25 years with only one tropical depression (in 1975). From 1995 to 2010, there were four hurricanes, three of which were category 4. Of particular interest are Hurricane Donna in 1960 (category 4, approaching from the northeast), Hurricane Omar in 2008 (category 4, approaching from the southwest), and Hurricane Earl in 2010 (category 4, approaching from the northeast). Subsequent to the historical period analysed, the category 5 Hurricane Irma, followed by the more distant category 3 Hurricane Maria, affected Anegada in September 2017.

Figure 5. Map of mean storm and hurricane frequency (events/year) for the North Atlantic, on which are superimposed tracks of hurricanes that have directly impacted Anegada. The name of the storm is displayed at the end of the storm track.

Figure 6. Storm and hurricane intensity from 1940 to 2010, and historical shoreline records: The size and colour of the top bar corresponds to the hurricane category, as in Figure 5. The name of the storm or hurricane is displayed on the top of the bar.

4.3. Wave Modelling

Figures 7–9 show the simulated wave height H (in m) and wave-induced force (in N/m^2) for fair-weather and selected extreme wave conditions. Since surge levels were not known, 0.5 m (the maximum tidal range) was added to the MSL for fair-weather and swell waves, while for storm conditions the surge level was set at 1 m, based on measured observations of a surge of this elevation on Anegada during Hurricane Earl (2010) [25].
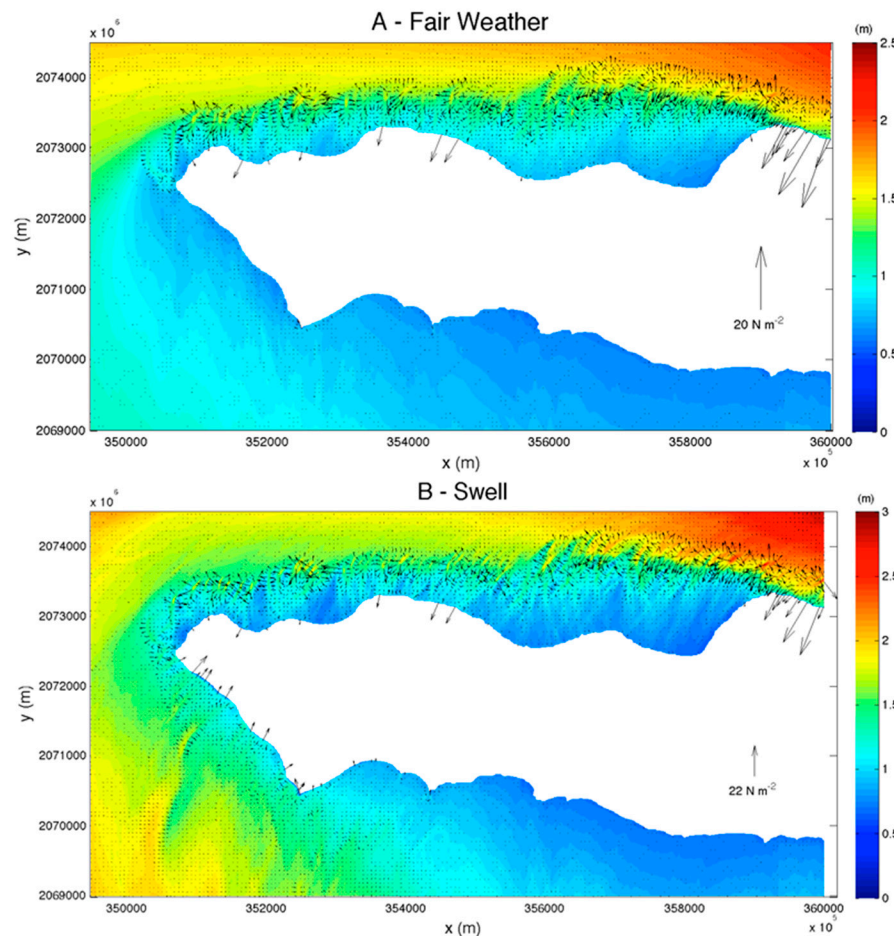
Figure 7. Simulated fair-weather (**A**) and swell (**B**) conditions models for west Anegada. The colour map represents the wave height H, and the arrows are the wave force direction and intensity.
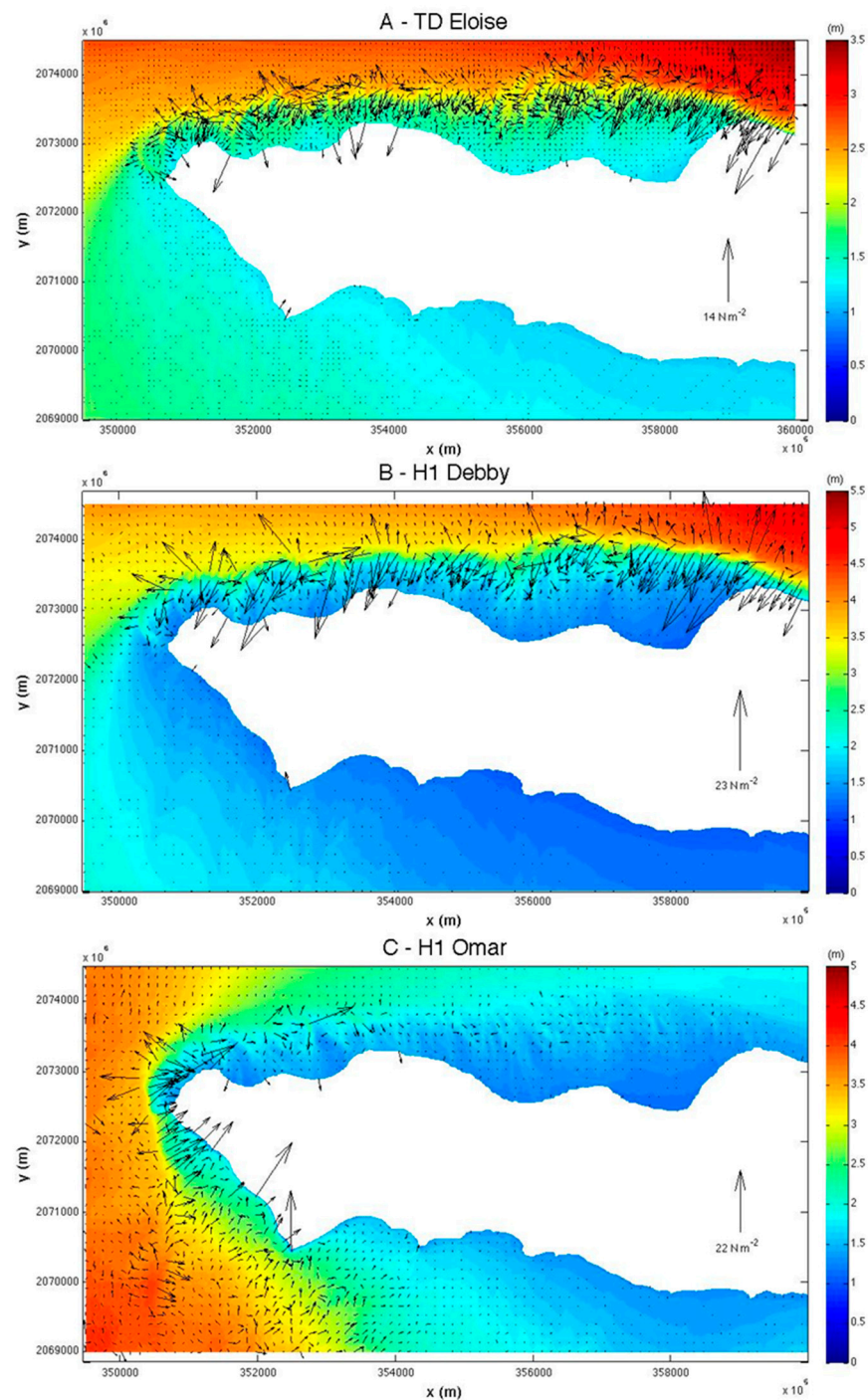
Figure 8. Tropical depression to category 1 hurricane model results for west Anegada. The colour map represents the wave height H, and the arrows are the wave force direction and intensity (length). (**A**) Tropical Depression Eloise (1975). (**B**) Category 1 Hurricane Debby (2000). (**C**) Category 1 Hurricane Omar (2008).

For fair-weather conditions (Figure 7A) and a ground swell event (Figure 7B) from east to northeast, the wave height drops markedly between the reef crest and the lagoon. The force vectors initially increase on the fringing reef and are then steered by the complex reef morphology. In the northern lagoon, the wave height is between 0.5 and 1.5 m for both fair-weather and swell conditions. For the fair-weather case, H is homogeneous in all parts of the lagoon, while the swell case shows higher H in front of the points and low H in front of the bays. For swell, zones of higher waves coincide with northeast–southwest-orientated

linear sandbanks in the lagoon (Figure 2). On the shoreline for both simulations, a few large force vectors are directed onshore, but most small vectors are directed offshore. At Soldier Point, the vector sizes and directions indicate the potential for overwash even for fair-weather or swell conditions. Despite the east–west island orientation and incoming northeasterly waves, wave crests behind the fringing reef are shore-parallel or swash-aligned. This is also evident along the southern shore. For fair-weather conditions on the southwest shore the waves are <<1 m, while for swell conditions H ranges between 1 and 2 m and many force vectors are directed onshore.
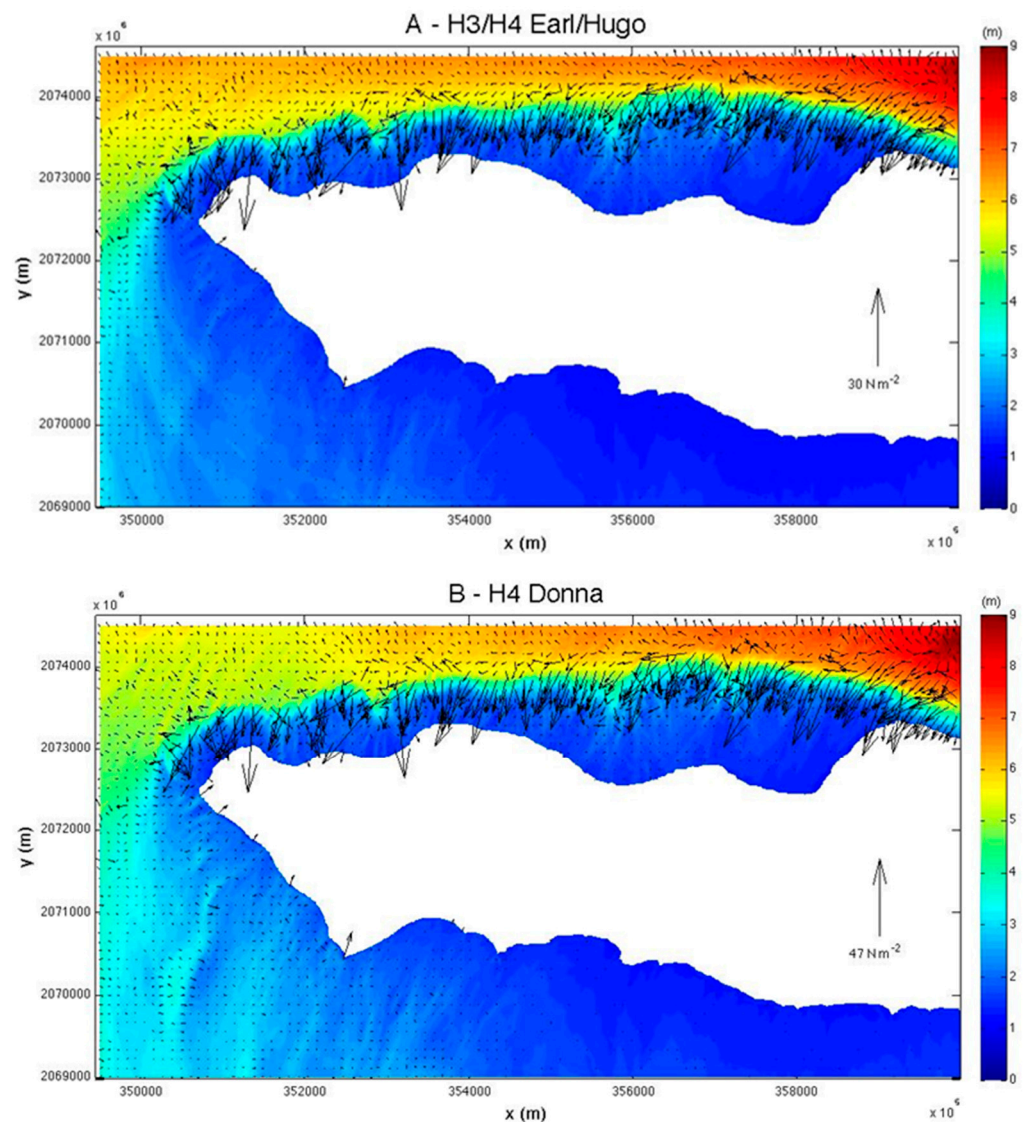
Figure 9. Category 3 and 4 hurricane models. The map represents the wave height H, and the arrows are the wave force direction and intensity. (**A**) Category 3–4 hurricane conditions like Hurricanes Earl (2010) and Hugo (1989, itself not affecting Anegada but the rest of the BVI (Hubbard, 1992) [8]). (**B**) Category 4 Hurricane Donna (1960) conditions.

Figure 8 shows the modelled wave conditions for three specific storm events, ranging from tropical depressions to category 1 hurricanes. These illustrate the conditions during Storm Eloise (1975 m, Figure 8A), Hurricane Debby (2000, Figure 8B), and Hurricane Omar (2008, Figure 8C). Debby and Omar had similar deep-water wave heights but different approach directions. Omar was unusual because it formed in the Caribbean Sea and ended in the central Atlantic. During Eloise (Figure 8A), although the reef represented a natural barrier to incoming east–northeast waves, H reached 1.5 m in the lagoon and along the

shorelines. The wave crests were shore-parallel on the north and southwest shorelines. During Debby (Figure 8B), the wave height reached 2.5 m in the northern lagoon and 1.5 m along the shoreline. The wave crests were shore-parallel. In contrast, during Hurricane Omar (Figure 8C), the wave height reached 2 to 2.5 m along the southwest shoreline. The force vectors were shore-normal and were the strongest simulated for the southern shore. The southwest incoming Omar waves affected the area from West End to Walkover Set Bay, but the northern shore was sheltered from their approach.

Waves during Hurricanes Earl (Figure 9A) and Donna (Figure 10B) both had an east–northeast wave approach and initial deep-water wave heights of 10 and 12 m, respectively. In the lagoon, the wave height (H) ranged from 1 to 3 m for both simulations. Wave-induced stress vectors over the fringing reef and in the lagoon were aligned northeast–southwest for both hurricanes.
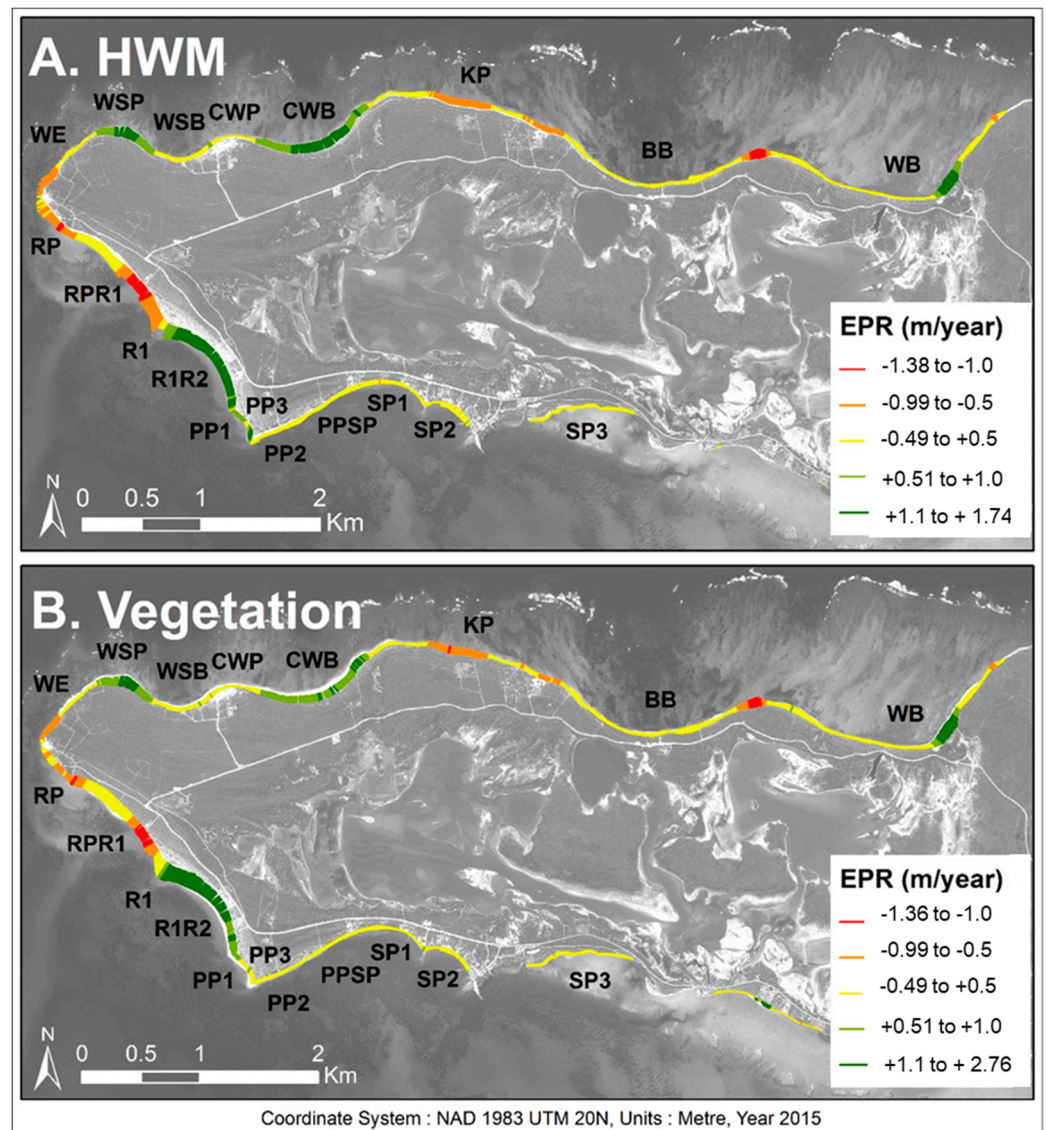

Figure 10. Shoreline changes for the HWM and the vegetation line. The length of each transect corresponds to the shoreline change envelope (in metres) of each of the shorelines. The colour scale corresponds to the end point rate (in metres/year; same class values for the two figures) for each type of shoreline, with a colour scale of red representing strong erosion, orange representing light erosion, yellow representing no changes, light green representing light accretion, and green representing strong accretion.

For all simulations, the wave heights were markedly reduced across the reef and the wave direction was modified. Whatever the incoming wave direction, the force vectors are shore-normal when they reach the north and southwest shorelines. Although wave-induced force simulations indicate a strong east–west drift along the northern shore, this is concentrated on the reef crest rather than the shoreline. The southwest shoreline has low-energy conditions except for the wind and wave conditions associated with Hurricane Omar. For fair-weather, swell, and storm conditions, distinct northeast–southwest-orientated zones of concentrated wave energy and enhanced force vectors develop in the lagoon and extend from the reef crest to the shoreline. They are best illustrated in the swell wave simulation (Figure 7B). Their orientation and location is consistent with elongated sand stringers that extend from the reef crest to the shoreline throughout the lagoon.

4.4. Historical Shoreline Change

The net shoreline changes are presented in Figure 10. The HWM and vegetation shoreline change results are similar, indicating that the beach width has remained consistent over time. The end point rates (EPRs) are displayed in Tables 6 and 7. The tables present the local minimum, maximum, average, and mean for each shoreline section.

Table 6. North coast sections' HWM end point rates from 1953 to 2009.

North Coast Section	Min	Max	Average	Median
WB (*n* = 243)	−0.69	1.47	0.24	0.18
BB (*n* = 179)	−1.36	0.41	−0.03	0.1
KP (*n* = 190)	−0.91	0.88	−0.35	−0.47
CWB (*n* = 110)	0.05	1.37	0.95	0.98
CWP (*n* = 27)	−0.04	0.53	0.15	0.04
WSB (*n* = 75)	0.16	1.12	0.56	0.48
WSP (*n* = 33)	0.14	1.31	0.8	0.89
WE (*n* = 63)	−0.82	0.47	−0.2	−0.19

Table 7. South coast sections' HWM end point rates from 1953 (only RP) or from 1959 to 2009 (all of the others).

South Coast Section	Min	Max	Average	Median
RP (*n* = 31)	−1.07	−0.49	−0.72	−0.7
RPR1 (*n* = 92)	−1.38	0.04	−0.55	−0.51
R1 (*n* = 42)	−0.86	1.74	0.31	0.48
R1R2 (*n* = 35)	0.98	1.63	1.35	1.35

Table 7. *Cont.*

South Coast Section	Min	Max	Average	Median
PP1 (*n* = 37)	0.4	1.24	0.7	0.61
PP2 (*n* = 38)	−0.29	0.01	−0.13	−0.14
PP3 (*n* = 22)	−0.12	1.31	0.35	0.01
PPSP (*n* = 106)	−0.52	0.31	−0.22	−0.18
SP1 (*n* = 28)	−0.05	0.34	0.11	0.1
SP2 (*n* = 30)	−0.17	0.18	−0.03	−0.04
SP3 (*n* = 88)	−0.43	0.25	−0.11	−0.13

Prominent progradation was evident in Windlass Bight, Cow Wreck Bay, Walkover Set Bay and Point, and from R1 to Pomato Point (Figure 10). Erosion was recorded at Keel Point and Bones Bight Point on the north shore and from West End to R1 on the southwest coast. The north coast is characterised by recession on the points and progradation in the embayments, with transitional sections in between. The southwest coast is clearly eroding in the west and accreting in the east around Pomato Point.

In Figure 11, the average net shoreline movement (NSM) and end point rate (EPR) of the HWM are shown for each of the six consecutive shoreline records. Each image shows shoreline changes between successive images. Despite gaps in the record due to cloud cover, some differences in temporal behaviour are evident. Windlass Bight shows progressive, unidirectional shoreline changes, while the coastline between Ruffling Point and Pomato Point alternates between strong progradation and strong recession.

Along the north coast, the shoreline behaviour alternates along the shore, with general recession on the points and progradation in the embayments (Figures 10–12). Windlass Bight and Bones Bight have complex temporal behaviour (Figure 11). Cow Wreck Bay was clearly prograding, while the shoreline at Keel Point was clearly receding for all three observable periods (1953–1966. 1992–2002. and 2002–2009). The section between West End and Pomato Point alternates between strong recession and strong progradation. The periods 1959–66 on the southwest coast and 1966–69 on the north coast show the greatest spatial extent of shoreline progradation.

Windlass Bight accreted significantly in its easternmost part between 1969 and 1992 (+83.18 m for the HWM and +86.48 m for the vegetation line). The central part was broadly stable and the western part of the bay also accreted (Figure 10). Recession in the central part between 1953 and 1960 was followed by moderate progradation (Figure 11). Bones Bight faces a shallow area of the lagoon. The shoreline shows strong recession in the east (Figure 10), while in the west it ranges from stable to moderate progradation. At the limit between Bones Bight and Keel Point there is a transition area with moderate recession in 1953–1992 and moderate progradation from 1992 to 2009.

The trend at Keel Point is one of consistent shoreline recession, with an EPR of −0.35 m/year for the HWM between 1953 and 2009 (Figures 10–12; Tables 6 and 7). The maximum net change between 1953 and 2009 was −56.5 m for the central part of the point. Although the year-to-year data for HWM are not complete, the change rates appear to be temporally variable. Between 1953 and 1966, the HWM retreated at −0.14 m/year. This increased to −0.95 m/year between 1992 and 2002, and then decreased. Landward of the most seaward set of beachridges at Keel Point, the 1966 and 1969 photos show an area of

bare sand (Figure 12) that had become vegetated by 1992. This appeared after the passage of Hurricane Donna in 1960, and it can be interpreted as Hurricane-generated overwash.
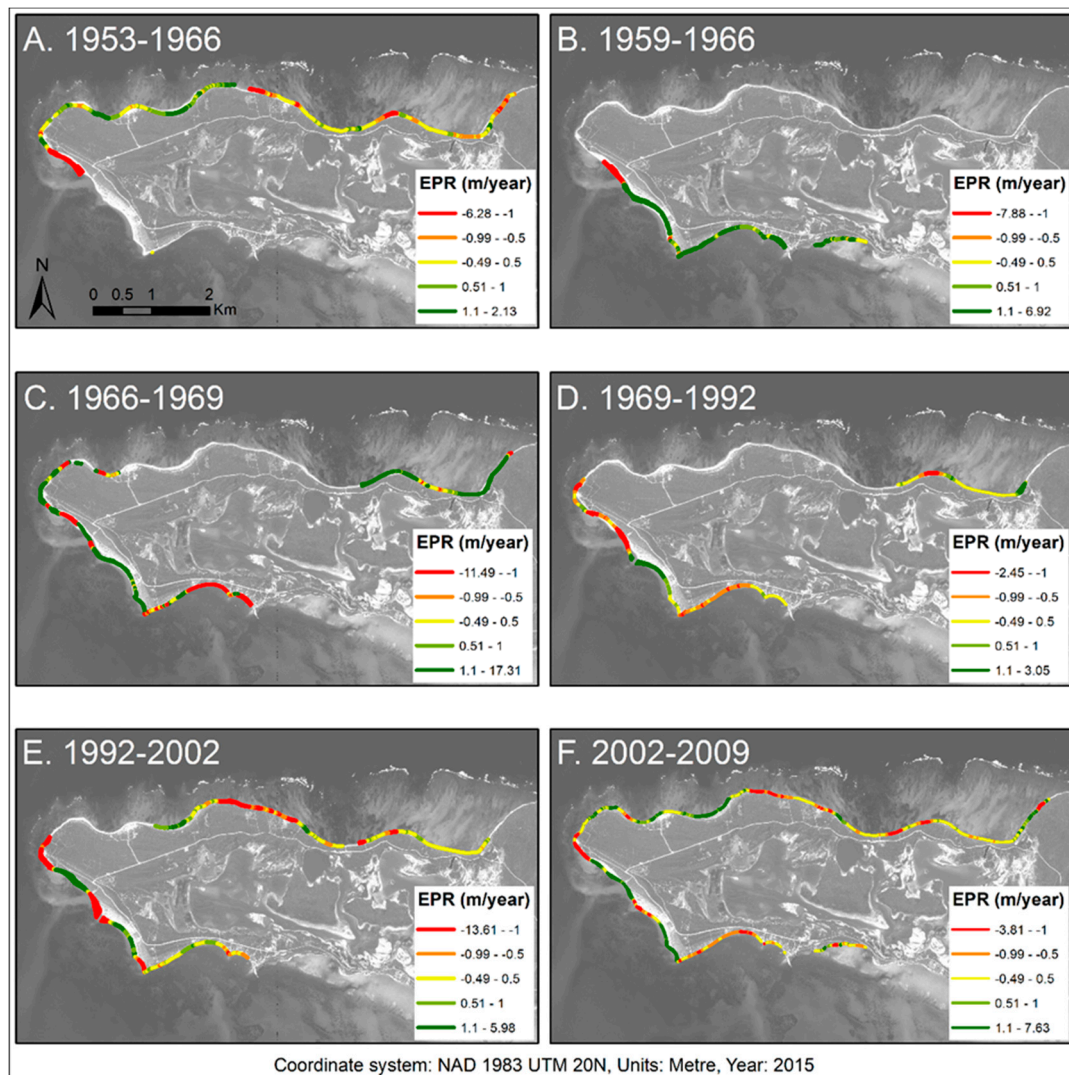

Figure 11. High-water mark SCE and EPR changes for all sections and all years. Same colour scale as Figure 9; only minimum and maximum values are changing. Note that the scale present on (A) is the same for all 6 images, and all of the changes are displayed on the 2009 satellite image.

Cow Wreck Bay shows extensive progradation (Figures 10–12). The median NSM for the vegetation line is +51.77 m. This progradational trend is broadly constant in the year-to-year analysis for the HWM (Figure 11) and the vegetation line. Cow Wreck Point shows little change in its eastern part (Figure 10). The western part, however, shows progradation that was confirmed to be continuing during 2015 fieldwork. Walkover Set Bay and Walkover Set Point show a similar general progradation trend for the period from 1953 to 2009 (Figures 10 and 11). The maximum progradation of the HWM is +62.2 m for the bay and +73.63 m for the point (Table 7). Some year-to-year datasets are missing for the HWM due to the poor quality of the aerial photos. Some recession is evident between 1953 and 1966 and between 1966 and 1969 (Figures 11 and 12). The trends are similar for the vegetation lines (Table 7): some recession is observed, but overall strong progradation is dominant. Moreover, the vegetation trend between 1992 and 2002 in Figure 11 for this area points to stabilisation of the shoreline. The West End section shows moderate progradation in the north and recession in the south (Figures 11 and 12). In the eroding area (from West End to Ruffling Point), initial progradation was followed by recession (Figure 11).
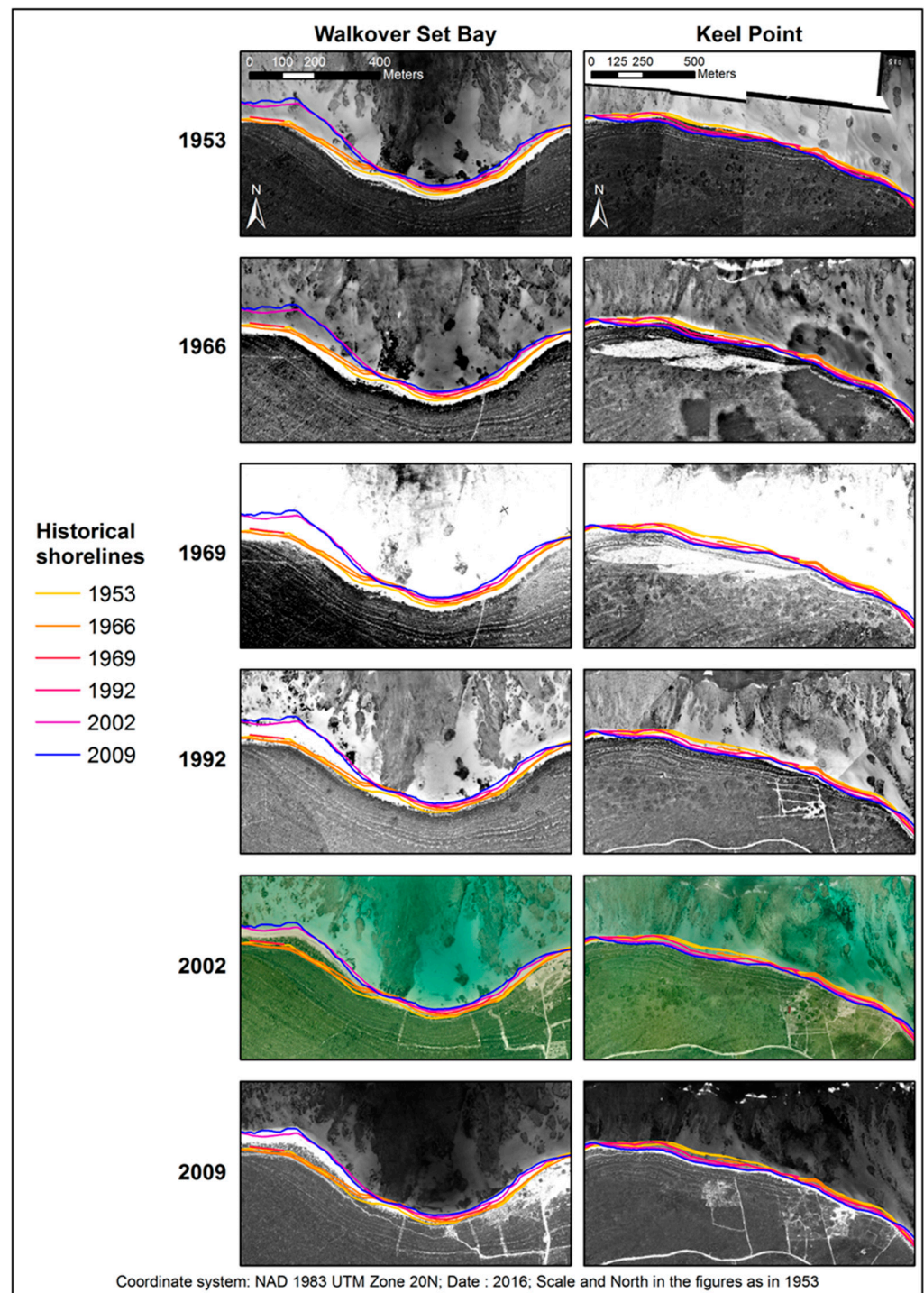
Figure 12. Shoreline changes at Walkover Set Bay and Keel Point during the study time. Note the washover fan appearing between 1953 and 1966 behind Keel Point.

The southwest coast from Ruffling Point to Pomato Point's cuspate foreland and then east to Settling Point (Figures 10–12) is the most dynamic in the study area. The 600 m long shoreline between Ruffling Point and R1 experienced recession from 1953/59 to 1992, followed by progradation up to 2009 (Figure 11). The adjacent shoreline (RPR1) of similar length shows numerous changes in rate and direction. These involve recession (1959 to 1966), stabilisation (1966 to 1969), progradation near the R1 point (1969–1992), recession (1992–2002), and renewed stabilisation between 2002 and 2009 (Figure 11). The HWM and vegetation line do not show the same temporal behaviour in this section: the vegetation lags

behind the shoreline progradation, indicating that stabilisation by vegetation is a slower process than sand accretion to the beach face.

The R1 point accreted and prograded to the east between 1969 and 1992 (Figure 11). After 1992, the cuspate foreland disappeared and the coastline became straighter. From R1 to R2, the coast exhibited only progradation from 1959 to 2009 (Figure 10, Figure 11). Then, from R2 to Pomato Point West (PP1 and PP3 in Tables 6 and 7), the shoreline advanced from 1959 to 1992, retreated from 1992 to 2002, and advanced back to the 1992 level by 2009. From Pomato Point East to Setting Point (PP2 and PPSP in Tables 6 and 7), the data are incomplete due to the quality of the aerial photos. In the first set (1959 to 1969) and second set (1992 to 2009), no major changes were observed. East of Settling Point, discontinuous mangroves occur.

5. Discussion

The drivers of shoreline changes at multidecadal timescales are complex and involve both dynamic (predominantly wave-forcing) and geological (e.g., sediment supply, antecedent topography) factors and their interactions [53,54]. As in most studies of multidecadal shoreline changes, information on relevant geological parameters is lacking for Anegada, and interpretation relies largely on the observation of linkages between dynamic forcing and morphological change. These then permit inferences regarding sediment supply and geological influences.

Anegada's geographical position exposes it to extreme waves of Atlantic and Caribbean origins. Storms can be particularly effective in alongshore redistribution of sand [55] and/or offshore transport [56]. Their impacts are strongly dependent on the trajectory of the storm relative to the coast [57,58], and they are not uniformly distributed in time. The study period contains two broad storminess intervals (Figure 5): a calm period from 1960 to 1995, and a period with multiple extreme wave events from 1995 to 2009. For the Atlantic Basin, the storm and hurricane activity periods have been linked to the position of the Atlantic Multidecadal Oscillation (AMO) and the North Atlantic Oscillation (NAO) [59], but also to the Madden–Julian Oscillation (MDO) [60] or the El Niño–Southern Oscillation (ENSO) [61]. Combined, the AMO and NOA cyclically drive the position of the hurricane corridor in the Caribbean and storminess in the North Atlantic. Strong hurricane activity happens when warm sea-surface temperatures (AMO-positive), mainly in the Western Atlantic, face a mild-to-cold humid Arctic winter (NAO-positive). This was the case for the end of the 20th century (1985 to 2003) [59], during which period only Hurricane Luis (1995) hit Anegada.

Since 2003, the combined positive AMO and negative NAO have been driven by a warm sea-surface temperature and low solar activity (i.e., cold winters in the Artic) [59]. This should result in more storms in the Atlantic Basin than over the Caribbean Sea, with extratropical cyclones reaching Northwestern Europe. Two hurricanes (Omar and Earl) impacted Anegada in 2008 and 2010, respectively. However, Omar was a hurricane that developed in the Caribbean Sea and headed east. Its formation was due to a combination of an easterly MDO and warm sea-surface temperatures. The easterly MDO drove the hurricane track east–northeast instead, directing it to the Gulf of Mexico. Finally, the hurricane season of 2017 saw two extreme hurricanes (Irma and Maria) crossing over or nearby Anegada. Although this study does not extend to these two events, they are consistent with the trend of increasing storminess since 2003.

The main direction of wave approach at Anegada is from the east (Figure 3) and east–northeast for storms and hurricanes (Figure 4). As the tidal range is minimal (under 0.5 m), wave energy is focused at the same level of the beach face, except during storm surges. Because the offshore transition of the reef edge is steep, storm surges are likely to be small. However, storm surges and swashes are high enough to leave a drift line above the maximum tide line. The steep slope and high bottom friction of the reef decrease incoming storm wave energy on the north coast. The easterly main wave direction drives a unidirectional longshore drift from biogenic sediment sources on Horseshoe Reef and the emergent Pleistocene section of the island. The transfer of sediment from the reef to

the shoreline appears to take place via linear zones of high wave energy (Figure 7) that traverse the lagoon under all simulated wave conditions. The orientation and extent of these zones are similar to sand stringers visible on satellite and air photographs (Figure 11) that extend from the reef crest across the lagoon to the sandy shoreline. The high degree of rounding and sorting of the beach's sand grains indicates that they have undergone significant abrasion and transport from the reef source.

Although both points and embayments have been subject to changes in shoreline position over the >50-year study period, their multidecadal persistence on this mobile sandy shoreline suggests that they are controlled by long-term topographic effects of the reef crest on incident waves. The long-term shoreline change results show three distinct morphodynamic domains (i.e., zones encompassing areas of similar multidecadal shoreline changes) in west Anegada (Figure 13):
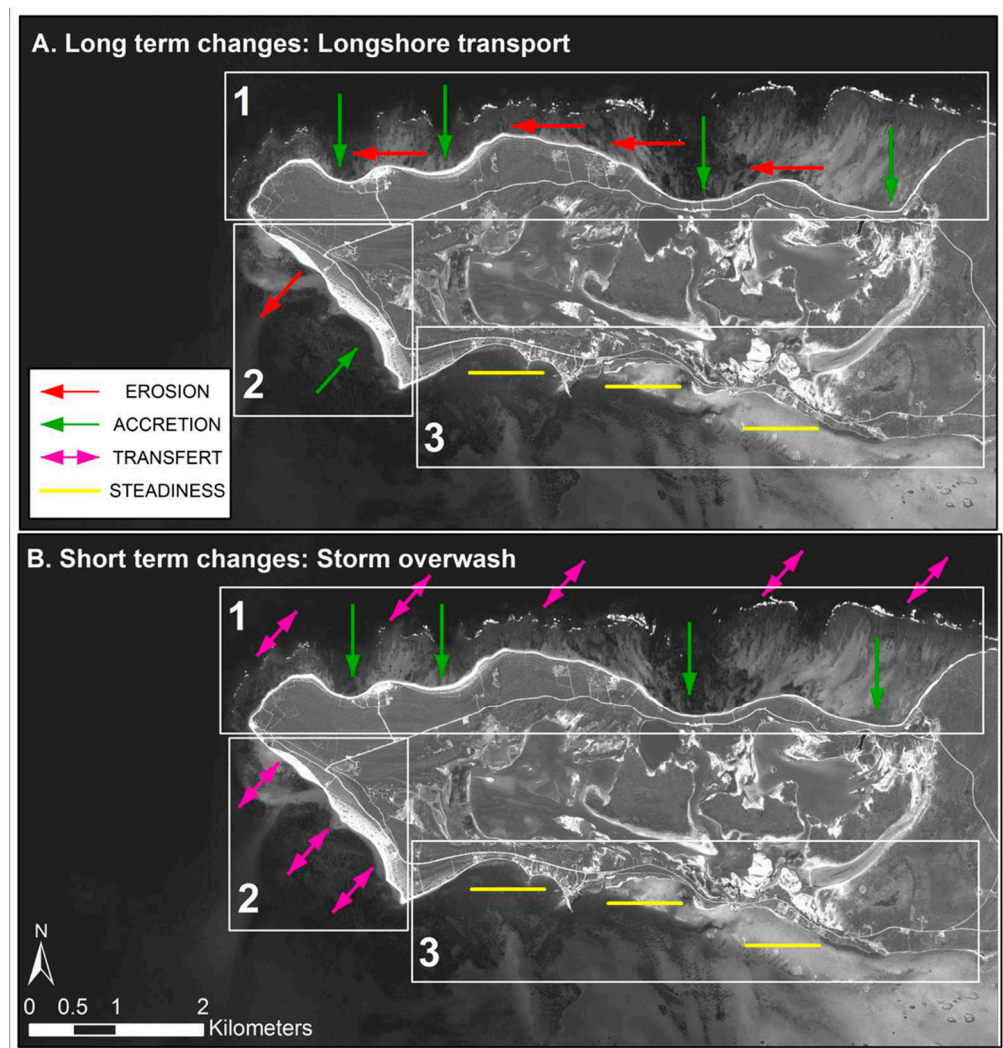

Figure 13. Long-term changes vs. short-term changes: (**A**) Longshore transport for west Anegada. (**B**) Storm overwash for west Anegada.

1. The north coast shows general shoreline progradation in the embayments and recession on the headlands;
2. The section from West End to Pomato Point shows strong temporal and spatial variability in shoreline behaviour, with spatially alternating recession and progradation;
3. East of Pomato Point, the shoreline shows little-to-no change.

These three behaviours are broadly consistent between 1953 and 2009, except for a period of more widespread progradation in the 1960s, when the frequency of storms was low.

Wave modelling suggests that storm events affect each of these zones in different ways. In the north, increased wave heights and wave-induced stress during storms intensify the longshore drift on the reef crest. The increased wave energy in the lagoon may be linked to sediment transfer from the points to the embayments, and storm run-up is able to deliver sediment to the supratidal zone to build shore-parallel beachridges. On the southwest shoreline, refraction of storm waves initiates periodic erosion and a southerly drift of sand that accumulates at Pomato Point. It is likely that some eroded sand accumulates in subtidal sand banks south of Anegada. These could act as a sediment source for subsequent storms approaching from the south or west. On the south coast, sheltered conditions permit the development of mangroves.

Wave modelling shows that much of the incident wave energy is intercepted and the force vectors are highly modified by the reef. There is also a clear difference in energy focusing and shoreline wave heights between fair-weather and storm conditions (Figure 13). Along the north shore, the embayments are generally accreting (Windlass Bight, Cow Wreck Bay, and Walkover Set Point Bay), while the points are generally eroding (Keel Point and Cow Wreck Point) (Figures 10–12). This implies the development of a series of coastal cells within which sediment is eroded and deposited. Cannibalisation of existing sediment from the points and accumulation in the intervening downdrift embayments is consistent with the implied east–west longshore drift and a trend toward straightening of the shoreline. Erosion at Keel Point, for example, appears to supply the fast-accreting downdrift shorelines at Cow Wreck Bay and Walkover Set Bay (Figures 10 and 11). Sand accretion at Windlass Bight and Bones Bight at the eastern end of the beachridge system implies sediment transport directly from the adjacent updrift reef and shoreline deposits and/or from the immediately fronting reef crest (1200 m wide) (Figure 2). The maturity of the beach sediment suggests abrasion and sorting consistent with longshore transport over a significant distance and/or time. This is supported by the shore-oblique wave energy vectors at Windlass Bight (Figures 7–9), while significant shoreline progradation is evident in the shoreline change analysis (Figures 10 and 11).

The presence of headlands suggests different formative conditions than those prevailing at present. The lack of storms from 1960 to 1995 (Figure 6) may have preferentially allowed accretion on the points. The period of storminess that started at the end of the 1990s is still ongoing due to the AMO and NDO variations, and this could have initiated the erosional trend at the points that was observed in the shoreline change analyses. However, reef morphology also affects island shorelines [62], and the position of the headlands could also be linked to breaks in the fringing reef (Figures 7–9). Near these reef breaks, the model results show that swell can increase and storm waves can reach the beach.

At West End, the shoreline changes to a northwest–southeast orientation. Here, easterly waves are refracted around the point to generate a southeast-directed longshore drift. The net shoreline trends point to loss of sediment from the northwest and accumulation in the southeast under the dominant refracted drift direction. However, the marked temporal variability in shoreline behaviour in this section indicates that sediment is periodically delivered to West End from the northern shoreline (causing local accretion), after which it is transferred toward Pomato Point or onto the Virgin Islands Bank (reflected in erosion at West End). The model results (Figures 7–9) show the importance of longshore sediment transport in this area. The dominant easterly waves have a limited effect on the south coast, where only swells and south-approaching storm waves affect the shoreline. On the south coast beyond Pomato Point, the shoreline changes are minor. The prevailing low wave energy on the Caribbean side of the island results in mangrove-fringed shorelines, highlighting the low wave energy there [63].

The observed multidecadal shoreline behaviour points to alongshore movement of sediment in a series of longshore cells whose position is controlled by the influence of the

reef crest on incident waves. The shoreline changes suggest a high degree of reworking of existing beach sediment along the shore. This is somewhat at odds with the long-term geomorphological evolution of the island. The multiple beachridges behind the modern shoreline suggest a strongly positive sediment budget for much of the island's existence, whereas cannibalisation of existing sediment is suggested in the past half-century. The inferred ongoing input of reef sediment to the beach via linear sand stringers thus appears to be less than the volume of sediment being transported along the shore and points to a contemporary negative sediment budget.

6. General Discussion

Globally, an estimated 100 million people benefit from risk reduction from the presence of a reef [9,64]. Coral reefs around Anegada reduce incoming waves' height and energy. The significant drop in wave height for all modelled conditions matches the 85–95% wave attenuation measured elsewhere [9,65].

Carbonate tropical islands are perceived to be at risk from global climate change [6], rising sea levels [3], and reef degradation [4]. The recorded shoreline changes at Anegada, however, point to an active sedimentary system involving carbonate sediment input from Horseshoe Reef, its transport along the north shore under longshore drift, and then rapid dispersal to the south side of Anegada or into subtidal shoals of the Virgin Islands Bank. In the mesoscale, this results in spatially and temporally variable rates of shoreline change in response to changes in energy input (moderated by storms).

The multidecadal shoreline change rates—both positive and negative—reported for Anegada are similar to those of other carbonate island shorelines [3,66–69], although the erosional and depositional areas on Anegada occur in close alongshore proximity, suggesting longshore linkages in sediment source and deposition. The majority of carbonate atoll islands are stable or accreting (i.e., increasing in area) [70], in spite of rising sea levels. This suggests the widespread existence of generally positive sediment budgets in carbonate-producing systems. The general accretionary status of Anegada over the course of the Holocene (as evidenced by its multiple beachridges) is similarly indicative of a strongly positive reef-derived sediment budget. However, shoreline changes in the past 50 years suggest a reduced sediment input and a switch to reworking and cannibalisation that may be linked to a reduction in reef sediment delivery.

On a fringing reef like Anegada, reef growth is vertical, creating little accommodation space for sediments on the reef itself [71]. Reefal sediments are instead transported ashore, forming the beachridge plain. The recurrence of extreme wave events influences the reef framework's development [72–74] and is essential to avoid reef burial by sediments in the long term, but it should not be too short, so as to avoid permanent damage [74]. The coral reef's biological state—living or dead—may influence its shoreline protection and sediment supply functions [74]. Caribbean reefs have been particularly threatened since 1970, and many are considered to be endangered [6,53,75], although Horseshoe Reef is in a moderate condition [18]. The shoreline change rates on Anegada are moderated by sediment supply and wave energy modification from this reef. The historical changes reported here may reflect a long-term change or a short-term low-sediment-supply interval that is not detectable in the multi-century record of beachridge plain evolution.

7. Conclusions

This study describes mesoscale shoreline changes around the beachridge plain of western Anegada island. The island is situated at the junction of two marine domains: Atlantic incoming extreme wave events impact the island regularly, while Caribbean Sea events are rare. A unidirectional longshore drift occurs along the north coast, related to the main incoming wave direction. This drives a large-scale westerly movement of carbonate sediments, especially on the reef crest, but also on the shoreline. Along the northern shore, longshore drift shifts sediment from east to west and results in the creation of a series of sediment cells, within which points are cannibalised to feed the embayments. A very active

zone at the southwest of the island reflects variations in sediment supply and dispersal from the northern shoreline. East of Pomato Point, the presence of mangroves is consistent with a low-energy, stable shoreline. A mechanism for carbonate sediment transfer from the reef crest to the shoreline is suggested by the development of linear zones of higher wave energy that coincide with sand stringers running obliquely across the lagoon.

Extreme wave events have affected the island at various times during the study period, and two broad storm regimes were identified—one calm period up to 1995, and a period of more regular and intense storm activity since then. Higher-energy storm events produce strong run-up along the shoreline in areas where beachridges form. A combination of reef-derived sediment supply and storm run-up is essential for beachridge formation.

Nearshore processes depend on the direction of approach of storms or hurricanes. In the north, as shown by the modelling, the fringing reef acts to strongly reduce incoming waves' energy and redirects the waves to a swash-aligned regime, creating a persistent configuration of points and embayments. This highlights the reef morphology's importance in the definition of Anegada's mesoscale coastal processes. In a climate change context with progressive reef decline, the future resilience of such tropical carbonate islands depends largely on the reef status for both sediment supply and wave protection. The historical changes observed suggest that the island may be shifting from a positive to a negative sediment budget. Whether this is the start of a long-term secular trend or a shorter-term fluctuation cannot be determined at present, but our results highlight the need for further investigation of linkages between reef status, carbonate sediment production, and sandy carbonate islands' stability in a climate change context.

References

1. Kench, P.S.; Cowell, P.J. Variations in sediment production and implications for atoll island stability under rising sea level, 2002. In Proceedings of the Ninth International Coral Reef Symposium, Bali, Indonesia, 23–27 October 2000; Volume 2, pp. 1181–1186.
2. Reguero, B.G.; Beck, M.W.; Agostini, V.N.; Kramer, P.; Hancock, B. Coral reefs for coastal protection: A new methodological approach and engineering case study in Grenada. *J. Environ. Manag.* **2018**, *210*, 146–161. [CrossRef] [PubMed]
3. Biribo, N.; Woodroffe, C.D. Historical area and shoreline change of reef islands around Tarawa Atoll, Kiribati. *Sustain. Sci.* **2013**, *8*, 345–362. [CrossRef]
4. Perry, C.T.; Kench, P.S.; Smithers, S.G.; Riegl, B.; Yamano, H.; O'Leary, M.J. Implications of reef ecosystem change for the stability and maintenance of coral reef islands. *Glob. Chang. Biol.* **2011**, *17*, 3679–3696. [CrossRef]
5. Scheffers, S.R.; Haviser, J.; Browne, T.; Scheffers, A. Tsunamis, hurricanes, the demise of coral reefs and shifts in pre-historic human populations in the Caribbean. *Quat. Int.* **2009**, *195*, 69–87. [CrossRef]
6. Eakin, C.M.; Morgan, J.A.; Heron, S.F.; Smith, T.B.; Liu, G.; Alvarez-Filip, L.; Baca, B.; Bartels, E.; Bastidas, C.; Bouchon, C.; et al. Caribbean corals in crisis: Record thermal stress, bleaching, and mortality in 2005. *PLoS ONE* **2010**, *5*, e13969. [CrossRef] [PubMed]

7. Cowell, P.J.; Thom, B.G. Morphodynamics of coastal evolution. In *Coastal Evolution: Late Quaternary Shoreline Morphodynamics*; Carter, R.W.G., Woodroffe, C.D., Eds.; Cambridge University Press: Cambridge, UK, 1994; pp. 33–86.

8. Hubbard, D.K. Hurricane-Induced Sediment Transport in Open-Shelf Tropical Systems—An Example from St. Croix, U.S. Virgin Islands. *J. Sediment. Res.* **1992**, *62*, 946–959.

9. Ferrario, F.; Beck, M.W.; Storlazzi, C.D.; Micheli, F.; Shepard, C.C.; Airoldi, L. The effectiveness of coral reefs for coastal hazard risk reduction and adaptation. *Nat. Commun.* **2014**, *5*, 3794. [CrossRef]

10. Roeber, V.; Bricker, J.D. Destructive tsunami-like wave generated by surf beat over a coral reef during Typhoon Haiyan. *Nat. Commun.* **2015**, *6*, 7854. [CrossRef]

11. Ford, M.R.; Kench, P.S. Multi-decadal shoreline changes in response to sea level rise in the Marshall Islands. *Anthropocene* **2015**, *11*, 14–24. [CrossRef]

12. Nunn, P.D.; Kohler, A.; Kumar, R. Identifying and assessing evidence for recent shoreline change attributable to uncommonly rapid sea-level rise in Pohnpei, Federated States of Micronesia, Northwest Pacific Ocean. *J. Coast. Conserv.* **2017**, *21*, 719–730. [CrossRef]

13. Testut, L.; Duvat, V.; Ballu, V.; Fernandes, R.M.; Pouget, F.; Salmon, C.; Dyment, J. Shoreline changes in a rising sea level context: The example of Grande Glorieuse, Scattered Islands, Western Indian Ocean. *Acta Oecologica* **2016**, *72*, 110–119. [CrossRef]

14. Duvat, V.K.; Salvat, B.; Salmon, C. Drivers of shoreline change in atoll reef islands of the Tuamotu Archipelago, French Polynesia. *Glob. Planet. Chang.* **2017**, *158*, 134–154. [CrossRef]

15. Tuck, M.E.; Ford, M.R.; Kench, P.S.; Masselink, G. Sediment supply dampens the erosive effects of sea-level rise on reef islands. *Sci. Rep.* **2021**, *11*, 5523. [CrossRef]

16. Romine, B.M.; Fletcher, C.H.; Barbee, M.M.; Anderson, T.R.; Frazer, L.N. Are beach erosion rates and sea-level rise related in Hawaii? *Glob. Planet. Chang.* **2013**, *108*, 149–157. [CrossRef]

17. Gore, S. Anegada: An Emergent Pleistocene Reef Island. In *Coral Reefs of the United Kingdom Overseas Territories*; Sheppard, C.R., Ed.; Springer: The Netherlands, 2013; pp. 47–60.

18. Dunne, R.P.; Brown, B.E. Some aspects of the ecology of reefs surrounding Anegada, British Virgin Islands. *Atoll Res. Bull.* **1979**, *236*, 1–80. [CrossRef]

19. Gore, S. Introduction to Reefs and Shorelines of the British Virgin Islands. In *Coral Reefs of the United Kingdom Overseas Territories*; Springer: Dordrecht, The Netherlands, 2013; pp. 23–35.

20. Peel, M.C.; Finlayson, B.L.; McMahon, T.A. Updated world map of the Köppen-Geiger climate classification. *Hydrol. Earth Syst. Sci.* **2007**, *11*, 1633–1644. [CrossRef]

21. Atwater, B.F.; Brink, U.S.T.; Buckley, M.; Halley, R.S.; Jaffe, B.E.; López-Venegas, A.M.; Reinhardt, E.G.; Tuttle, M.P.; Watt, S.; Wei, Y. Geomorphic and stratigraphic evidence for an unusual tsunami or storm a few centuries ago at Anegada, British Virgin Islands. *Nat. Hazards* **2010**, *63*, 51–84. [CrossRef]

22. Gore, S. Beach Geomorphology and Management in the British Virgin Islands. Ph.D. Thesis, University of Ulster, Coleraine, UK, 2012.

23. Gore, S.; Cooper, J.A.G.; Jackson, D.W.T.; Jarecki, L. Spatial variability in beach biogeomorphology in a tropical archipelago. *Earth Surf. Process. Landf.* **2019**, *44*, 1860–1875. [CrossRef]

24. Clubbe, C.; Gillman, M.; Acevedo-Rodríguez, P.; Walker, R. Abundance, distribution and conservation significance of regionally endemic plant species on Anegada, British Virgin Islands. *Oryx* **2004**, *38*, 342–346. [CrossRef]

25. Atwater, B.F.; Fuentes, Z.; Halley, R.B.; Brink, U.S.T.; Tuttle, M.P. Effects of 2010 Hurricane Earl amidst geologic evidence for greater overwash at Anegada, British Virgin Islands. *Adv. Geosci.* **2014**, *38*, 21–30. [CrossRef]

26. Watt, S.; Buckley, M.; Jaffe, B. Inland fields of dispersed cobbles and boulders as evidence for a tsunami on Anegada, British Virgin Islands. *Nat. Hazards* **2011**, *63*, 119–131. [CrossRef]

27. ReefBase. ReefBase: A Global Information System for Coral Reefs. Available online: http://www.reefbase.org (accessed on 20 January 2022).

28. Cooper, J.A.G.; Jackson, D.W.T.; Gore, S. A groundswell event on the coast of the British Virgin Islands: Spatial variability in morphological impact. *J. Coast. Res.* **2013**, *65*, 696–701. [CrossRef]

29. Dorville, J.-F.; Zahibo, N. Storm surge induced by hurricane Omar on the Caribbean coasts, example of the port of Deshaies in Guadeloupe. *Geophys. Res. Abstr.* **2009**, *11*, 1103.

30. Zahibo, N.; Pelinovsky, E.; Yalciner, A.C.; Kurkin, A.; Koselkov, A.; Zaitsev, A. The 1867 Virgin Islands Tsunami. *Nat. Hazards Earth Syst. Sci.* **2003**, *3*, 367–376. [CrossRef]

31. Atwater, B.F.; Brink, U.S.T.; Cescon, A.L.; Feuillet, N.; Fuentes, Z.; Halley, R.B.; Nuñez, C.; Reinhardt, E.G.; Roger, J.H.; Sawai, Y.; et al. Extreme waves in the British Virgin Islands during the last centuries before 1500 CE. *Geosphere* **2017**, *13*, 301–368. [CrossRef]

32. Reinhardt, E.G.; Pilarczyk, J.; Brown, A. Probable tsunami origin for a Shell and Sand Sheet from marine ponds on Anegada, British Virgin Islands. *Nat. Hazards* **2011**, *63*, 101–117. [CrossRef]

33. Cordrie, L.; Feuillet, N.; Gailler, A.; Biguenet, M.; Chaumillon, E.; Sabatier, P. A Megathrust earthquake as source of a Pre-Colombian tsunami in Lesser Antilles: Insight from sediment deposits and tsunami modeling. *Earth—Sci. Rev.* **2022**, *228*, 104018. [CrossRef]

34. Gardner, T.A.; Côté, I.M.; Gill, J.A.; Grant, A.; Watkinson, A.R. Hurricanes and Caribbean Coral Reefs: Impacts, Recovery Patterns, and Role in Long-Term Decline. *Ecology* **2005**, *86*, 174–184. [CrossRef]

35. US National Oceanographic and Atmospheric Administration. Buoys Data Centre. Available online: http://www.ndbc.noaa.gov (accessed on 1 September 2014).

36. Grothe, P.R.; Taylor, L.A.; Eakins, B.W.; Carignan, K.S.; Caldwell, R.J.; Lim, E.; Friday, D.Z. Digital Elevation Models of the U.S. Virgin Islands: Procedures, Data Sources and Analysis. In *NOAA Technical Memorandum NESDIS NGDC-55*; U.S. Department of Commerce: Boulder, CO, USA, 2012; p. 50.

37. National Oceanic and Atmospheric Administration. Historical Hurricane Tracks. Available online: http://coast.noaa.gov/hurricanes/ (accessed on 1 March 2015).

38. BVI Government. *Unpublished Nautical Charts Data*; BVI Government: British Virgin Islands, UK, 2013.

39. Collin, A.; Hench, J.L. Towards deeper measurements of tropical reefscape structure using the WorldView-2 spaceborne sensor. *Remote Sens.* **2012**, *4*, 1425–1447. [CrossRef]

40. Loureiro, C.; Ferreira, Ó.; Cooper, J.A.G. Extreme erosion on high-energy embayed beaches: Influence of megarips and storm grouping. *Geomorphology* **2012**, *139*, 155–171. [CrossRef]

41. Booij, N.; Holthuijsen, L.H.; Ris, R.C. The SWAN wave model for shallow water. In Proceedings of the 25th International Conference on Coastal Engineering, Orlando, FL, USA, 2–6 September 1996; pp. 668–676.

42. Nelson, R. Hydraulic roughness of coral reef platforms. *Appl. Ocean Res.* **1996**, *18*, 265–274. [CrossRef]

43. Monismith, S.G.; Rogers, J.S.; Koweek, D.; Dunbar, R.B. Frictional wave dissipation on a remarkably rough reef. *Geophys. Res. Lett.* **2015**, *42*, 4063–4071. [CrossRef]

44. Sheppard, C.; Dixon, D.J.; Gourlay, M.; Sheppard, A.; Payet, R. Coral mortality increases wave energy reaching shores protected by reef flats: Examples from the Seychelles. *Estuar. Coast. Shelf Sci.* **2005**, *64*, 223–234. [CrossRef]

45. Fonseca, M.A.; Fisher, J.S. A comparison of canopy friction and sediment movement between four species of seagrass with reference to their ecology and restoration. *Mar. Ecol. Prog. Ser.* **1986**, *29*, 15–22. [CrossRef]

46. Pajak, M.J.; Leatherman, S. The high water line as shoreline indicator. *J. Coast. Res.* **2002**, *18*, 329–337.

47. Fisher, J.S.; Overton, M.F. Interpretation of Shoreline Position from Aerial Photographs. In Proceedings of the 24th Conference on Coastal Engineering, Kobe, Japan, 29 January 1994; Volume 24, pp. 1998–2003.

48. Boak, E.H.; Turner, I.L. Shoreline Definition and Detection: A Review. *J. Coast. Res.* **2005**, *214*, 688–703. [CrossRef]

49. Rogers, S.S.; Sandweiss, D.H.; Maasch, K.A.; Belknap, D.F.; Agouris, P. Coastal Change and Beachridges along the Northwest Coast of Peru: Image and GIS Analysis of the Chira, Piura, and Colan Beach-Ridge Plains. *J. Coast. Res.* **2004**, *20*, 1102–1125. [CrossRef]

50. Thieler, E.R.; Himmelstoss, E.A.; Zichichi, J.L.; Ergul, A. *Digital Shoreline Analysis System (DSAS)—An ArcGIS Extension for Calculating Shoreline Change, version 4.0*; Open-File Report; U.S. Geological Survey: Reston, VA, USA, 2008; p. 1278.

51. Spiske, M.; Pilarczyk, J.E.; Mitchell, S.; Halley, R.B.; Otai, T. Coastal erosion and sediment reworking caused by hurricane Irma–implications for storm impact on low-lying tropical islands. *Earth Surf. Process. Landf.* **2022**, *47*, 891–907. [CrossRef]

52. Spiske, M.; Halley, R.B. A coral-rubble ridge as evidence for hurricane overwash, Anegada (British Virgin Islands). *Adv. Geosci.* **2014**, *38*, 9–20. [CrossRef]

53. Hamon-Kerivel, K.; Cooper, A.; Jackson, D.; Sedrati, M.; Pintado, E.G. Shoreface mesoscale morphodynamics: A review. *Earth-Sci. Rev.* **2020**, *209*, 103330. [CrossRef]

54. Cooper, J.; Green, A.; Loureiro, C. Geological constraints on mesoscale coastal barrier behaviour. *Glob. Planet. Chang.* **2018**, *168*, 15–34. [CrossRef]

55. Morton, R.A.; Gibeaut, J.C.; Paine, J.G. Meso-scale transfer of sand during and after storms: Implications for prediction of shoreline movement. *Mar. Geol.* **1995**, *126*, 161–179. [CrossRef]

56. Plant, N.G.; Flocks, J.; Stockdon, H.F.; Long, J.W.; Guy, K.; Thompson, D.M.; Cormier, J.M.; Smith, C.G.; Miselis, J.L.; Dalyander, P.S. Predictions of barrier island bermevolution in a time] varying storm climatology. *J. Geophys.—Cal Res. Earth Surf.* **2014**, *119*, 300–316. [CrossRef]

57. Otvos, E.G. Hurricane signatures and landforms-toward improved interpretations and global storm climate chronology. *Sediment. Geol.* **2011**, *239*, 10–22. [CrossRef]

58. Guisado-Pintado, E.; Jackson, D.W.T. Multi-scale variability of storm Ophelia 2017: The importance of Synchronized environmental variables in coastal impact. *Sci. Total Environ.* **2018**, *630*, 287–301. [CrossRef]

59. Van Vliet-Lanoë, B.; Penaud, A.; Hénaff, A.; Delacourt, C.; Fernane, A.; Goslin, J.; Hallégouët, B.; Le Cornec, E. Middle-to late-Holocene storminess in Brittany (NW France): Part II—The chronology of events and climate forcing. *Holocene* **2014**, *24*, 434–453. [CrossRef]

60. Maloney, E.D.; Hartmann, D.L. Modulation of hurricane activity in the Gulf of Mexico by the Madden-Julian oscillation. *Science* **2000**, *287*, 2002–2004. [CrossRef]

61. Donnelly, J.P.; Woodruff, J.D. Intense hurricane activity over the past 5000 years controlled by El Niño and the West African monsoon. *Nature* **2007**, *447*, 465. [CrossRef] [PubMed]

62. Kench, P.; Parnell, K.; Brander, R. Monsoonally influenced circulation around coral reef islands and seasonal dynamics of reef island shorelines. *Mar. Geol.* **2009**, *266*, 91–108. [CrossRef]

63. Mazda, Y.; Magi, M.; Kogo, M.; Hong, P.N. Mangroves as a coastal protection from waves in the Tong King delta, Vietnam. *Mangrove sSalt Marshes* **1997**, *1*, 127–135. [CrossRef]

64. Quataert, E.; Storlazzi, C.; van Rooijen, A.; Cheriton, O.; van Dongeren, A. The influence of coral reefs and climate change on wave-driven flooding of tropical coastlines. *Geophys. Res. Lett.* **2015**, *42*, 6407–6415. [CrossRef]

65. Brander, R.W.; Kench, P.S.; Hart, D. Spatial and temporal variations in wave characteristics across a reef platform, Warraber Island, Torres Strait, Australia. *Mar. Geol.* **2004**, *207*, 169–184. [CrossRef]

66. Restrepo, J.C.; Otero, L.; Casas, A.C.; Henao, A.; Gutiérrez, J. Shoreline changes between 1954 and 2007 in the marine protected area of the Rosario Island Archipelago (Caribbean of Colombia). *Ocean Coast. Manag.* **2012**, *69*, 133–142. [CrossRef]

67. Ford, M. Shoreline changes interpreted from multi-temporal aerial photographs and high resolution satellite im-ages: Wotje Atoll, Marshall Islands. *Remote Sens. Environ.* **2013**, *135*, 130–140. [CrossRef]

68. Webb, A.P.; Kench, P.S. The dynamic response of reef islands to sea-level rise: Evidence from multi-decadal analysis of island change in the Central Pacific. *Glob. Planet. Chang.* **2010**, *72*, 234–246. [CrossRef]

69. Johnston, W.; Cooper, J.; Olynik, J. Shoreline change on a tropical island beach, Seven Mile Beach, Grand Cayman: The influence of beachrock and shore protection structures. *Mar. Geol.* **2023**, *457*, 107006. [CrossRef]

70. Duvat, V.K.E. A global assessment of atoll island planform changes over the past decades. *WIREs Clim. Chang.* **2018**, *10*, e557. [CrossRef]

71. Kennedy, D.; Woodroffe, C. Fringing reef growth and morphology: A review. *Earth-Sci. Rev.* **2002**, *57*, 255–277. [CrossRef]

72. Blanchon, P.; Richards, S.; Bernal, J.P.; Cerdeira-Estrada, S.; Ibarra, M.S.; Corona-Martínez, L.; Martell-Dubois, R. Retrograde Accretion of a Caribbean Fringing Reef Controlled by Hurricanes and Sea-level Rise. *Front. Earth Sci.* **2017**, *5*, 91–108. [CrossRef]

73. Perry, C.T.; Spencer, T.; Kench, P.S. Carbonate budgets and reef production states: A geomorphic perspective on the ecological phase-shift concept. *Coral Reefs* **2008**, *27*, 853–866. [CrossRef]

74. Rogers, C.S. Hurricanes and coral reefs: The intermediate disturbance hypothesis revisited. *Coral Reefs* **1993**, *12*, 127–137. [CrossRef]

75. Aronson, R.; Precht, W. Conservation, precaution, and Caribbean reefs. *Coral Reefs* **2006**, *25*, 441–450. [CrossRef]